CrystEngComm

Accepted Manuscript

ROYAL SOCIETY OF CHEMISTRY

www.rsc.org/crystengcomm

Growth and characterization of 6-chloro-2, 4-dinitroaniline crystals in anti-solvent precipitation and reprecipitation methods

Rajaboopathi Mani[a,b], Krishnakumar Varadharajan[b*], Marjatta Louhi–Kultanen[a*]

[a]Department of Chemical Technology, Lappeenranta University of Technology, Lappeenranta 53851, Finland

[b]Department of Physics, Periyar University, Salem 636 011, India

Abstract

The presence of superstructure and impact of solvent on the formation of different forms in simple trimorphic system of 6-chloro-2, 4-dinitroaniline (CDA) are investigated in this report. The experiment was carried out as part of sorting three forms in CDA. The form I and form III were obtained in anti-solvent precipitation method. The filtrate, i.e. the mother liquor obtained from anti-solvent precipitation was further used in slow evaporative crystallization experiment. This evaporation method yielded superstructures on form I crystals in acetone (primary solvent) and water (secondary solvent). The obtained results showed that superstructures on form I resulted in by combining anti-solvent crystallization and slow evaporative crystallization. Reprecipitation method was carried out to verify the observed superstructure on form I at different volume fractions of water. Furthermore, superstructure was observed in slow evaporation of CDA solution in acetone-water mixture. The solubility data were measured for CDA in pure acetone, ethyl acetate (EtOAc), dichloromethane (CH_2Cl_2), methyl *tert*-butyl ether (MTBE) and binary acetone-water, CH_2Cl_2-MTBE, EtOAc-MTBE solvent mixture at 293 K and 298 K. X-ray powder diffraction study confirms the formation of different forms and recorded SEM images lay a foundation for understanding the origin of superstructure. The functional group vibrations and packing difference between form I and form III were clearly identified from the FTIR spectra. The UV-Vis-NIR results confirmed the interaction between water and solute in solution. Based on the solvent parameters and SEM images, the formation of superstructure was hypothesized.

Keywords: Crystal growth; Polymorphism; Solubility; Organic mesocrystals; FTIR; UV-Vis-NIR.

*** Corresponding authors' email:**

(1) vkrishna_kumar@yahoo.com, Tel. +91 427-2345766 Extn: 246, Fax: +91 427-2345565.

(2) marjatta.louhi@lut.fi, Tel.+358 40 701 8078, Fax +358 5 621 2199.

1. Introduction

The solvent composition plays an important role to control the supersaturation, crystal nucleation and growth rate in crystal growth process [1]. The different forms of polymorphic crystal are obtained based on different solvents and this strategy plays a vital role in pharmaceutical crystallization [2]. This report discusses the crystal growth and characterization of polymorphism of 6-chloro-2, 4-dinitroaniline (CDA) in anti-solvent precipitation, reprecipitation and slow evaporation solution growth technique (SEST). The different forms were characterized by using various analytical tools such as XRPD, FTIR, SEM, UV-Vis-NIR and thermal analysis. Further, we have explored the formation of superstructure on form I in CDA crystals. In anti-solvent precipitation method, the anti-solvent i.e. precipitant or secondary solvent is added into solution to reduce solubility of solute in original solvent and consequently generate a supersaturation driving force for crystal nucleation. The rate of supersaturation is highly dependent on addition rate of anti-solvents and mole fraction of solvents used for crystal growth. This method is widely used in pharmaceutical industries [3]. Reprecipitation is a facile method to prepare the organic nanocrystals [4]. To date, much strategy has been developed to optimize the morphology, size and properties of crystals based on solvent composition, solubility and addition method. The Reprecipitation involves a rapid mixing of stock solution, which is prepared by dissolving solute in a good solvent and excess amount of secondary solvent. The great disparity in solubility between two solvents and good miscibility are essential in this method [5-7]. An addition of precipitant into solution at particular rate (anti-solvent; semi-batch process) and direct addition of solution into precipitant (reprecipitation; batchwise) are the differences between anti-solvent precipitation and reprecipitation methods. In addition to that, the amount of solvent and precipitant used in both methods are different. In our investigations, water and MTBE were used as a secondary solvent in these methods. Further, an attention has been paid to understand the impact of secondary solvent and formation of superstructure or mesocrystals on form I.

Mesocrystals are referred as a superstructure of crystalline nanoparticle with external crystal faces on the scale of some hundred nanometers to micrometer [8]. The formation of mesocrystal is a non-classical event in which more than one-step of aggregation and fusion of building blocks form energetically a hierarchical structure on the crystal surface [9]. It can also be referred that an adsorption of molecules followed by subsequent diffusion across the crystal surface leads to form steps and kink sites consequently produce the flake built spherical

aggregations [10]. The morphology of mesocrystal is not similar to primary crystal symmetry. The identification of guiding force to form a mesocrystal is still in its infancy but several mesocrystal properties are known [8]. Lots of work has been reported on the self-assembly of low dimensional (0D -2D) and three-dimensional (3D) nanoparticle such as dendrites and hierarchical architecture in inorganic materials [11-15]. However, the formation mechanism of three-dimensional mesocrystal is merely reported. The difficulty in formation is due to high lattice energy of the inorganic materials, which leads to form single crystals rather than 3D superstructure [16]. The mesocrystal in organic materials has been a subject of research interest in recent years.

The advantage of superstructure in organic crystal is that mechanism of superstructure formation can be identified based on molecular interactions [17]. The flower shaped hierarchial structure of flake-built formation is uncommon in organic crystals. In 2007, Nakanishi *et al*. presented a hypothesis on the formation of flower like morphology grounded with observation of microscopic images of fullerene-based molecules during the growth. π stacked and van der Waals interactions are the initial driving force for the formation of mesocrystals in fullerene derivatives [18]. In 2009, Wang *et al.* reported the observation of superstructure in oligoarene derivatives via solution drop-casting process. The authors concluded that different flower like morphologies are due to different molecular conformations [19]. Recently, Ying Su *et al.* reported a flake-built spherical aggregations and dispersive flakes of diphenylalanine in reprecipitation method using different solvents [9]. It is to be noted that this molecule has already shown three low dimensional nanostructures such as nanotubes, nanofibrils and nanowires in different growth methods [20]. The observed flake-built aggregations possess 20 μm in diameter and quite similar to flower in shape. The length of the 2D petal is several micrometers and thickness is about 100 nm. The mechanism has been hypothesized based on solubility result of different solvents at various temperatures [9]. According to their results, the morphology of flower shape is temperature dependent and formation of hierarchical structure is due to miscibility of poor solvent with pre-dissolved solution of good solvent.

CDA is a trimorphic form, which shows three forms concomitantly in solution growth technique. The crystals possess different functional groups that involve different interactions in the crystal structure, which leads to produce different forms structurally different (form-I, P21/c; form-II, P21; and form-III, PI) from one another. The form II is needle in morphology and the

other forms are visually indistinguishable. These two forms were sorted based on mechanical properties by using layered crystal structure, and short axis distance [21]. Bag *et al.* argued the structure based assessment of mechanical properties of CDA and its suitability for tabletability [2]. Recently, we have reported the crystal growth of form II and form III in melt growth technique [22]. The noncentrosymmetric molecular arrangements of form II show high second harmonic generation conversion efficiency. There is no report for pseudomorphism in CDA. Our initial aim was to sort the different forms of CDA crystals using anti-solvent crystallization method. However, based on the result of superstructure formed in slow evaporation of filtrate in anti-solvent method and to diversify the understanding of superstructure formation on form I, reprecipitation method was carried out in this report. The superstructure formation in acetone-water mixed solvent in SEST method endorses the observed superstructure in slow evaporation of filtrate in anti-solvent method.

2. Experimental

2.1. Anti-solvent precipitation

Crystallization of CDA was performed by adding water as anti-solvent for solute, to acetone (from here on, AS_1) and MTBE as anti-solvent for solute, to CH_2Cl_2 (from here on, AS_2) and EtOAc (from here on, AS_3) solutions. Anti-solvent of 2 ml was added into 8 ml of CDA solution using a peristaltic pump at the rate of 0.2 ml min^{-1} (0.8-CDA volume fraction). The different solutions were prepared in acetone, CH_2Cl_2 and EtOAc. The experiment was also carried out for 0.6 volume fraction of acetone at 0.2 and 0.4 ml min^{-1} addition rates (from here on, AS_{12}). The anti-solvent was added at the fixed position of impeller near to the solution in order to maintain the motion of drop-wise solvent on the surface of stirred solutions. The formed precipitates were filtered out immediately after the addition of water and MTBE in acetone and CH_2Cl_2 solution respectively. The filtrates (rest of the solution after the precipitation) obtained from AS_1 and AS_2 were subjected to slow evaporation. The amount of precipitate obtained from the acetone (from here on, AS_{P1}) solution was low compared with dichloromethane (from here on, AS_{P2}) solutions. Since there was no precipitate formed in EtOAc solution during anti-solvent addition, the prepared solution was directly put into slow evaporation. The single crystals were obtained from the filtrate of AS_1 (from here on, AS_{C1}), AS_2 (from here on, AS_{C2}) and EtOAc-MTBE (from here on, AS_{C3}) solutions after 8-13 days.

2.2. Reprecipitation

In reprecipitation method, we followed two ways of adding stock solution into different volume fractions of water. In first method, the saturated CDA solution of acetone (3 ml) was prepared and injected rapidly into vigorously stirred water (10 ml) by using a syringe. The volume fraction of water in the solution was 0.76. Two other solutions with 0.83 and 0.86 volume fractions of water were also prepared. In second method, the saturated CDA solution of acetone (5 ml) was added directly into vigorously stirred water (10 ml). The volume fraction of water in the solution was 0.66. The volume fractions of water with 0.75 and 0.8 were also prepared. The precipitates obtained from the first (from here on, RP_1) and second (from here on, RP_2) methods were used for all the characterizations.

2.3. Slow Evaporation Solution Growth Technique (SEST)

The saturated solution of CDA was prepared in solvent mixture of acetone and water at the ratio of 4:1. The solution was filtered out using Whatman filter paper. The filtrate was covered with perforated foil and it was subjected to slow evaporation. The optically transparent single crystal of CDA was obtained after 7-10 days.

3. Solubility Study

CDA purchased from Sigma Aldrich was used without further purification for solubility measurement. The solvents used in the experiment were analytical grade purchased from Sigma Aldrich and Merck. The solubility measurement was carried out based on preparation of saturated solution followed by concentration determination (gravimetric method) at particular temperature. Hermetic metal box equipped with magnetic stirrer was used for solubility measurement. Temperature was controlled through thermostat (LAUDA RC-6 CP) with accuracy of ±0.05 K. An excess amount of solute was added into 5 ml of pure solvent, and the solution was stirred continuously using a magnetic stirrer at required temperature in the thermostat. The volume fraction of primary solvents (Acetone, EtOAc and CH_2Cl_2) is 0.8 in the case of mixed solvent i.e. 1 ml of secondary solvent was added into 4 ml of primary solvent. A period of 24 h was provided to ensure the solid–liquid equilibrium established in the solution. Then the stirring was stopped, and 2 ml of clear solution was sampled with preheated syringe near to the solution temperature. Acrodisc syringe filter with 0.2 μm PTFE membrane was used to filter the saturated CDA solution. The amount of solute dissolved in the solution was calculated by measuring the weight of the glass vessel, with and without solution. Complete evaporation of solvent was ensured

during the measurement. All the experiments were repeated two times at 293 K and 298 K temperatures. The saturated mole fraction solubility (χ^e) of CDA in pure and mixed solvent can be calculated from the following equation [23].

$$x^e = \frac{m_1/M_1}{m_1/M_1 + m_2/M_2 + m_3/M_3}, \qquad (1)$$

where m_1, m_2, and m_3 represent the masses of solute, primary and secondary solvent in the solutions. The molecular weights of solute, primary and secondary solvent in the solutions are denoted as M_1, M_2 and M_3 . The result of mole fraction solubility of CDA at 293 K and 298 K is presented in Table 1. The relative uncertainty of the experimental solubility values was less than 0.01. The result to emerge from the table is that the solubility of CDA in acetone was very high compared with other solvents. Further, addition of water has reduced the solubility of CDA in acetone about 75-80%. The reduction of solubility was 20-25% for CH_2Cl_2 and 10-15% for EtOAc for the addition of MTBE.

4. Results and Discussion

4.1. X-Ray Powder Diffraction

X-ray powder diffraction data were collected on a Rigaku Mini Flex II diffractometer using Cu Kα radiation (λ=1.54056 Å) at 20 kV over the 2θ range of 10-60˚ and scan rate at 5˚min^{-1}. Mercury 2.3 programme was used to generate the XRPD pattern from single crystal XRD data of CDA as an input [24, 21]. The precipitates obtained from the anti-solvent experiment AS_{P1} and AS_{P2} were used as such for diffraction measurement. The crystalline samples AS_{C1}, AS_{C2}, and AS_{C3} were gently grounded and then used for diffraction measurement. The recorded XRPD pattern is presented in Figure 1. The XRPD pattern of AS_{P1} and AS_{P2} was consistent with each other. These patterns were similar with the pattern of form I of CDA. The XRPD pattern of AS_{C3} was consistent with form III of CDA. The characteristic peaks of form I are 15˚7'±2', 16˚56'±2', and 21˚62'±2' (Figure 1S, see supplementary informations). These peaks are clearly distinct and not overlapped or interfered with other forms. These peaks were observed at 15˚72', 16˚68'±2' and 21˚62' for AS_{P1} and it is shown in Figure 1. The characteristic peaks of form III are 17˚76', 19˚08', 20˚58', 23˚4', 28˚58', 32˚34' and 36˚72'. Even though, the peaks are characteristic in nature, the position of the peaks are very close to the characteristic and common peaks of all other forms (Figure 1S). The characteristic peaks of form III were observed at 17˚.7', 19˚.06', 20˚.66', 23˚.46', 28˚.58', 32˚.34' and 36˚.7' for AS_{C3} (Figure 1). The characteristic peak of form I was observed at

16˚56' in form III. This indicates that minor amount of form I is contaminated in AS_{C3}. The form II was mainly dominated in AS_{C2}. However, other forms were also presented occasionally. It is to be noted that precipitate from AS_{P2} (CH_2Cl_2) was consistent with form I (acetone). This is contrary to the experimental result of form II obtained in CH_2Cl_2 [2]. Further, it is important to note that AS_{P1} and AS_{P2} were quite pure, and minor amount of other forms were presented in AS_{C1} and AS_{C2}. The XRPD plots of AS_{C1} and AS_{C2} are presented in Figure 2S.

The XRPD plot of precipitate obtained from reprecipitation method is presented in Figure 2. We observed only form I in RP_1 at the volume fraction of 0.76. Surprisingly, Form II was also observed along with form I at 0.83 and 0.86 volume fractions in RP_1. The same trend was observed in RP_2. However, the presence of form II was considerably low at 0.75 and 0.8 volume fractions compared with RP_1 (Figure 3S). These results are further confirmed by SEM images.

XRPD plot of crystals obtained in slow evaporation solution growth technique (SEST) is presented in Figure 4. The measurement was carried out for both crystalline and powder (after grinding) samples. The XRPD pattern of form I generated from single crystal data was similar with the pattern of crystals grown in SEST [21]. However, shift in peaks were observed for 2θ at 14˚84', 25˚66', 39˚38' and 56˚72'. These peaks were shifted to lower angles (14˚66', 25˚56', 38˚98' and 56˚52') for crystal grown in SEST. These lower angles shift were not uniform for all the peaks. On the other hand, uniform shift to lower angle in 2θ was observed for all the peaks observed in grounded sample compared with crystalline one. This shift may be due to formation of residual stress in the sample during mechanical grinding. Further, it is important to note that form I has already proven as a high plasticity material (shearing) compared with other forms in CDA during tabletability measurement [2].

4.2. FTIR Vibrational Spectra

The FTIR spectra are used as one of the important tools to distinguish the polymorphic forms in which different forms possess different interactions and that can be reflected in the vibrational spectrum. In last two decades, many studies have been reported to distinguish the pharmaceutical polymorphism using vibrational spectroscopy [25-27]. The frequency shifts, relative intensities, and number of bands are the observed differences among the different forms. These disparities in the spectra are due to difference in molecular packing result in different interactions in the crystal unit cells [28]. The FTIR spectra were recorded at KBr phase in the frequency region of 400-4000

cm^{-1} using PerkinElmer spectrometer at a resolution of 4 cm^{-1}. In sample preparation, ~3 mg of sample was grounded with ~250 mg KBr using mortar and pestle and pressed with metal die to prepare the pellet. The FTIR spectra of form I (AS_{P1}) and form III (AS_{C3}) of CDA are shown in Figure 4. The vibrational assignments of form I and form III corresponding to their functional group vibrations are presented in Table 2. *NH_2 Vibrations*; The medium intense peaks in the regions 3520-3420 cm^{-1} and 3420-3340 cm^{-1} are generally due to asymmetric and symmetric vibrations of primary aromatic amine [29]. These vibrations were observed at 3429 cm^{-1} and 3326 cm^{-1} for form I and 3447 cm^{-1} and 3337 cm^{-1} for form III. It is to be noted that form I vibrations are red shifted compared to form III. The NH_2 deformation vibration is expected to appear as strong band in the region 1650-1580 cm^{-1} [29]. This vibration was observed at 1627 cm^{-1} for form I and 1617 cm^{-1} for form III (red shifted). Due to conjugation effect between the lone pair of electron of nitrogen with benzene ring, C-N stretching vibrations are observed as two bands at 1360-1250 cm^{-1} and 1280-1180 cm^{-1}. These bands were observed at 1325 cm^{-1} and 1275 cm^{-1} for form I and 1328 cm^{-1} and 1276 cm^{-1} for form III. However, the band at 1328 cm^{-1} was strongly absorbed compared with other bands. Aniline has weak to medium intense band at 445-345 cm^{-1} due to in-plane bending vibration of NH_2 group. This vibration was observed above and below 400 cm^{-1} for electron accepting and donating substituent in the aniline. *NO_2 Vibrations:* The asymmetric and symmetric stretching vibrations of NO_2 group in aromatic compounds are generally observed at 1570-1485 cm^{-1} and 1370-1320 cm^{-1} respectively. These vibrations were observed at 1581 cm^{-1} and 1505 cm^{-1} for form I whereas 1591 cm^{-1} and 1505 cm^{-1} for form III. The intensity of symmetric vibration was increased due to electron donating substituent in the CDA crystals [30, 31]. Further, the doublet in symmetric region was due to conjugation effect of nitro group substitution in the benzene ring. The strong band at 740 cm^{-1} and 540 cm^{-1} was assigned to NO_2 in-plane deformation. Since NO_2 is an electron-donating group, this vibration was observed at 429 cm^{-1} for form I and 425 cm^{-1} for form III. *C-H and C=C Vibrations;* The C-H stretching vibration was observed as strong to medium intense band at 3097 cm^{-1} for form I and 3087 cm^{-1} for form III. The C=C stretching vibration was assigned to 1456 cm^{-1} and 1415 cm^{-1} for form I whereas 1461 cm^{-1} and 1417 cm^{-1} for form III. The region at 1290-900 cm^{-1} is generally assigned to C-H in plane pending of the aromatic ring. This band was observed at 1145 cm^{-1} and 1066 cm^{-1} for form I whereas 1154 cm^{-1} and 1081 cm^{-1} for form III. The absorption peak was sharp in lower frequency regions whereas strong and broad in higher frequency regions. The

changes in these regions indicate that inter or intra molecular interactions in the two forms are different due to packing polymorphism [29]. Further, it is important to note that aromatic C-H group plays a dominant role in hydrogen bond formation, resulting in different packing of polymorphs in CDA [21]. The C-H out of plane vibration was observed at 900-800 cm^{-1} [32]. The aromatic ring in plane and out of plane vibration was observed at 700-620 cm^{-1}. *C-Cl Stretching Vibrations;* The strong absorption band at 760-505 cm^{-1} is generally assigned to C-Cl stretching vibration. The band at 741 cm^{-1} was assigned to C-Cl stretching vibration of both forms. This band may possibly to appear in high frequency region due to vibrational coupling of Cl atom with other groups.

4.3. SEM

JEOL JSM-5800 Scanning Electron Microscopy (SEM) was used to examine the crystals grown by anti-solvent precipitation, filtrate and reprecipitation methods. The samples were fixed on a metal stud using carbon tape and the sample studs were dried under vacuum. The prepared samples were covered by approximately 10 nm gold coating. Figure 5(a, b) shows the image of precipitate obtained in AS_{P1}. The recorded SEM image shows that crystals has no sharp edges and possess some notches on the surfaces. It can be evidenced from the inset picture in Figure 5. The image of precipitate obtained in AS_{P2} is shown in Figure 5(c, d). The appearances of crystals are the same as the image of form I but smaller in size. It further supports the result of formation of form I in CH_2Cl_2 (AS_{P2}). It is to be mentioned that form II is obtained in CH_2Cl_2 in fast evaporation method [2]. It can be cleared from Figure 5 that growth rate of crystals in AS_{P1} was higher than AS_{P2} with in short span of time after the addition of precipitant. Surprisingly, we observed that the AS_{C1} crystals show hierarchical structure on the edges of form I by routine SEM measurements. This superstructure is a kind of "mesocrystals" (abbreviated as mesoscopically structured crystals) [33]. This flower like superstructure consists of hundreds of 2D square petals with length and width of several micrometers. The thickness of the petals is about 100 nm. Figure 6(a, b) shows the image of superstructure formed in AS_{C1}. This superstructure not observed in AS_{C3} is presented in Figure 7. The crystals of flat and smooth surfaces were constructed by multiple stacking of thin layers or terraces in nature [9]. From the SEM images of form I and form III, it can be confirmed that the morphology of form I and form III are not same. However, these two forms grown in slow evaporation method using CH_2Cl_2 are appeared the same and visually indistinguishable by naked eye [21].

The image of crystals grown at 0.6 volume fraction with different addition rates of water in AS_{12} gives shed light on further insight into the superstructure. Instead of appearing superstructure on the edges of crystal surfaces, we could observe this structure for 0.4 ml min^{-1} addition rate on the region where the assembly of rugged surface of the crystals. The recorded SEM image is presented in Figure 8(a, b). Further, the interlocked flake built form of superstructure was observed clearly is shown in Figure 8c. We have observed that the thickness of the petals is relatively high and buds in size at addition rate 0.2 ml min^{-1} for AS_{12} (Figure 4S). The observed changes in superstructure at 0.8 and 0.6 volume fractions are due to changes in solution composition and corresponding changes in the crystal-solution interfacial energy [34]. There was no considerable difference in the XRPD pattern as the quantity of superstructure was relative very low. From the SEM images, it can be concluded that the rugged or uneven surfaces of crystals are the origin for the formation of superstructure. Further details are given in section 5.

The SEM images of precipitate obtained in RP_1 are shown in Figure 9. We have expected that good miscibility of acetone-water and strong solute-water interaction, assist to form a micro-sized crystal covered with superstructure. In addition to that, instantaneous exposure of secondary solvent in acetone solution induces the supersaturation and it can possible to encompass the superstructure on the micro-sized crystal [9]. Conversely, we observed the smoothly faceted crystals without any superstructure in RP_1 at 0.76 volume fraction. However, at 0.83 volume fraction, surprisingly we have observed that, form I along with plenty of form II needle crystals. The same trend was observed at 0.86 volume fraction. Further, we could observe the similar result for volume fraction of water at 0.66 (form I), 0.75 and 0.8 (mixture) in RP_2. The crystal obtained in RP_2 is presented in Figure 5S. The amount of needle crystal in RP_2 was comparatively less with RP_1. It suggests that way and amount of addition of saturated CDA solution into the secondary solvent control the formation of form II crystals. It emerges from the images of Figure 9 and Figure 5S, the way and amount of addition of saturated solution has direct impact on the level of supersaturation for the formation of different forms [35, 7].

The SEM images of crystals grown from SEST method are presented in Figures 10 and 11. The superstructure observed in SEST method was similar with superstructure formed in slow evaporation of mother liquor in anti-solvent precipitation (AS_{C1}). However, the amount of formation of superstructure on form I in SEST method is relatively high compared with AS_{C1}. A deep understanding between anti-solvent precipitation and mixed solvent in SEST method is

important as it involves two solvents in both methods. The addition of water or secondary solvent in anti-solvent precipitation reduces the solubility of saturated solution result in supersaturation achieved for crystal growth. Further, the amount of precipitation in anti-solvent method is proportional to the amount of addition of secondary solvent and solubility difference between two solvents. On the other hand, the function of mixed solvent in SEST method decreases the solubility of solvent for crystal growth. The supersaturation is achieved by lowering the solution temperature in mixed solvent. Even though, the mother liquor in anti-solvent precipitation and mixed solvents in slow evaporation technique contain stoichiometric amount of acetone and water, the differences in formation of superstructure are clearly observed in Figures 6 and 10. The superstructure was not only observed in vertex and edges of the crystals, it was also observed in surface of the crystals. Furthermore, a kind of microsized kinks (the half-crystal molecular configurations where new molecules join the lattice) was observed in edges and surfaces of the crystals. The formation of kink may be initial step or origin for the formation of superstructure [36, 39]. The kinks are indicated by arrow and circle in Figure 11. The observed kinks are not smoothened and rod in shape.

4.4. UV-Vis-NIR Spectrum

The functional group interaction with solvent used in the growth process also affects the morphology of final products [18]. Absorption spectrum was recorded in Jasco V-670 spectrometer. The spectra were measured for AS_{P1} (form I) and AS_{C3} (form III). To identify the effect of solvent interaction, the spectra were taken for pure (acetone, EtOAc) and mixed solvents (acetone-water, EtOAc-MTBE). The ratio of mixed solvent was 4:1. The recorded spectra are presented in Figure 12. There was no change in the absorption peaks for form III in pure EtOAc and mixed (EtOAc-MTBE) solvents. On the other hand, changes were observed in form I for pure acetone and mixed (acetone-water) solvents, which indicates that the presence of solute-water interaction in the CDA solution.

5. **Possible Mechanism based on Solvent Parameters and SEM Images.**

Based on the properties of solvent, solubility and SEM images, we suggest the causes for the formation of superstructure in AS_{C1}. As mentioned in the introduction, solubility difference of CDA in different solvents and good miscibility are considered to be important for the formation of superstructure. Li *et al.* divided the solvents into three category based on different morphologies (flake, tube and fiber) of diphenylalanine obtained in different solvents. We take

into account the important solvent parameters such as Hildebrand and Scott's solubility parameter (δ), Gutman's electron acceptor number (AN) and electron donor number (DN) to describe the formation of superstructure [9]. The properties of solvents used in the experiments are presented in Table 3. Water has high δ value compared with other solvents used in the experiments. This indicates that cohesive energy density (square root of ratio of heat of vaporization and molar volume) required to separate the solvent molecules from one another is higher than other solvents, i.e. water has high intermolecular attractive force. Further, the high electron acceptor number (AN) reflects that the solute-water interaction is high compared with solute-MTBE interaction, almost absence in the UV absorption spectrum (Figure 12). Further, water can act as a hydrogen bond acceptor solvent due to its high AN value [9]. Since NH_2 group in aniline is a hydrogen bond donor group, the water molecules can have stronger interaction with NH_2 than NO_2 group. This interaction is evidenced in Figure 12 for AS_{C1}. We believe that good miscibility of acetone and water and strong interaction of solute-water assist to form a superstructure in crystals [9]. Further, atomically rough crystal faces have high density of kink sites. The supersaturated solution is thermodynamically favour for any adatom (adsorbed atom) arriving at a kink sites [35]. Instead of this site to involve in the formation of steps (new layers), the high density of kink sites leads to favour a fast growth rate and consequently form a superstructure [40]. Figure 5a further confirms the formation of superstructure at the uneven or rugged surfaces. The irony of result in reprecipitation method suggests that though water or secondary solvent cover the microenvironment of acetone solution instantly, the span of time to induce the superstructures may be less. However, this less time is sufficient to induce the nucleation of form II in RP_1 at the volume fraction of water higher than 0.76. The solubility of CDA in acetone may be less for the formation of superstructure in reprecipitation method. The growth of new form via cross nucleation in concomitant polymorphism (CDA) is straight forwarded; further investigations forward in this direction may be helpful to discover the fourth form in CDA crystals.

6. Conclusions

We firstly reported the observation of superstructure on form I by slow evaporation of filtrate from anti-solvent and slow evaporation solution growth technique (SEST). The acetone and water were used as a primary and secondary solvents for anti-solvent precipitation and mixture of these solvents were used for SEST method. The absence of form II at 0.76 and 0.66 volume fractions of water and presence of mixture of form II and form I above these volume

fractions were observed in reprecipitation method. The form II in reprecipitation method was controlled by different amounts of saturated CDA solutions. The solubility of CDA in acetone was high compared with other solvents used for the measurements. Solubility of CDA was reduced about 75-80% for 1 ml addition of water into 4 ml of CDA solution in acetone. This solubility reduction was about 20-25% in CH_2Cl_2 and 10-15% in EtOAc for 1 ml addition of MTBE. XRPD plot confirmed that the precipitate obtained during the addition of water into acetone in anti-solvent precipitation (AS_{P1}) was form I. The crystals grown from solvent mixture of EtOAc and MTBE was form III (AS_{C3}). The mixture of form I and form II at different volume fractions of water in reprecipitation methods were also confirmed. The observed frequency shift of C-H in-plane bending in aromatic ring indicates the different types of inter or intra molecular interaction presented in two forms. Further, the electron donating substitution in CDA was ascertained through symmetry vibration of NO_2 and in-plane bending vibration. The superstructure formed on form I and mixture of form I and form II in reprecipitation were evidenced from SEM images. The interaction of water with CDA in acetone solution was confirmed through absorption spectrum of CDA in acetone and acetone-water mixture. The strong solute water interaction and uneven or rugged surfaces on the crystal were the reason for the formation of superstructure in form I.

Acknowledgement

The author Rajaboopathi Mani thanks Indo-Finnish Government Scholarship Pool 2012-2013 for financial support under postgraduate exchange programme. The authors also thank for financial support of Academy of Finland (project 260141) and Lappeenranta University of Technology, Finland.

References

[1] C. J. Brown and X. Ni, Cryst. Growth Des., 2011, **11**, 719.

[2] P. P. Bag, M. Chen, C. C. Sun and C. M. Reddy, Cryst. Eng. Comm., 2012, **14**, 3865.

[3] N. Doki, N. Kubota, M. Yokota, S. Kimura and S. Sasaki, J. Chem. Eng. Jpn, 2002, **35**, 1099.

[4] H. Kasai, H. S. Nalwa, H. Oikawa, S. Okada, H. Matsuda, N. Minami, A. Kakuta, K. Ono, A. Mukoh and H. Nakanishi, Jpn. J. Appl. Phys. 1992, **31**, L1132.

[5] X. Holmback and A. C. Rasmuson, J. Cryst. Growth., 1999, **198–199**, 780.

[6] Z. Q. Yu, R. B. H. Tan and P. S. Chow, J. Cryst. Growth., 2005, **279**, 477.

[7] M. Kitamura and S. Hironaka, Cryst. Growth Des., 2000, **6**,1214.

[8] H. Colfen and M. Antonietti, Angew. Chem. Int. Ed., 2005, **44**, 5576.

[9] Y. Su, X. Yan, A. Wang, J. Fei, Y. Cui, Q. He and J. Li, J. Mater. Chem., 2010, **20**, 6734.

[10] W. K. Burton, N. Cabrera and F. C. Frank, Philos. Trans. R. Soc. Lond. A, 1951, **243**, 299.

[11] Q. Gong, X. Qian, X. Ma and Z. Zhu*, Cryst.Growth Des.,* 2006, **6**, 1821.

[12] Y. Sun, L. Wang, X. Yu and K. Chen, Cryst. Eng. Comm., 2012, **14**, 3199.

[13] C. Gua, J. Huang, Y. Wua, M. Zhaia, Y. Sunc and J. Liu, J. Alloys Compd., 2011, 509, 4499.

[14] W. Zhang, L. Shi, K. Tang and Z. Liu, Mater. Res. Bull., 2012, **47**, 1725.

[15] M. Yang and J.He, J. Colloid Interface Sci., 2012, **368**, 41.

[16] R. L. Penn and J. F. Banfield, Geochim. Cosmochim.Acta, 1999, **63**, 1549.

[17] C, Helmut and M. Antonietti, Angew. Chem. Int. Ed., 2005, **44**, 5576.

[18] T. Nakanishi, K. Ariga, T. Michinobu, K. Yoshida, H. Takahashi, T. Teranishi, H. Mohwald and D. G. Kurth, Small, 2007, **3**, 2019.

[19] L. Wang, Y. Zhou, J. Yan, J. Wang, J. Pei and Y. Cao, Langmuir, 2009, **25**, 1306.

[20] X. H. Yan, P. L. Zhu and J. B. Li, Chem. Soc. Rev., 2010, **39**, 1877.

[21] C. M. Reddy, S. Basavoju and G. R. Desiraju, Chem. Commun., 2005, 2439.

[22] V. Krishnakumar, M. Rajaboopathi, J. Therm. Anal. Calorim, 2014, **115**, 723.

[23] Q. Yu, X. Ma, L. Xu, ThermochimicaActa, 2013, **551**, 78.

[24] C. F. Macrae, I. J. Bruno, J. A. Chisholm, P. R. Edgington, P. McCabe, E. Pidcock, L. Rodriguez-Monge, R. Taylor, J. van de Streek and P. A. Wood, J. Appl. Cryst., 2008, **41**, 466.

[25] S. Wishkerman, and J. Bernstein, Cryst. Eng. Comm, 2006, **8**, 245.

[26] W. P. Findlay and D. E. Bugay, J. Pharm. Biomed.Anal., 1998, **16**, 921.

[27] M. C. Etter, Acc. Chem. Res. 1990, **23**, 120.

[28] M. Donahue, E. B. Sehic, D. Wells, C. W. Brown, American Pharm. Rev., 2011, **14**, 104.

[29] G. Socrates, Infrared and Raman Characteristic Group Frequencies, 3rd Edn. John Wiley & Sons, England, 2001.

[30] B. Lakshmaiah and G. R. Rao. J. Raman Spectrosc. 1989, **20**, 439.

[31] D. L. Hoghes and J. Trotter, J. Chem. Soc A. 1971, **0**, 2181.

[32] M. Margoshes andV. A. Fassel, SpectrochimicaActa, 1955–1956, **7**, 14.

[33] H. Colfen and M. Antonietti, Angew. Chem., Int. Ed., 2005, **44**, 5576.

[34] A.A. Chernov, P.N. Segre, A.M. Holmes, in Crystallization Physics in Biomacromolecular Solutions, ed. G. Muller, J.-J. Metois and P. Rudolph, Elsevier, Amsterdam, 1st edn.,2004, ch.1, pp. 109.

[35] Y. S. Zhao, H. Fu, A. Peng, Y. Ma, D. Xiao, J. Yao. Adv. Mater. 2008, 20, 2859.

[36] Encyclopedia, http://encyclopedia2.thefreedictionary.com/Crystal+formation (accessed December 2013).

[37] Virginia Tech, http://www.geochem.geos.vt.edu/bgep/pubs/Chapter_3_DeYoreo_Vekilov.pdf (accessed December 2013).

[38] Sebastian Wohlrab, Nicola Pinna, Markus Antonietti, and Helmut Colfen, Chem. Eur. J. 2005, 11, 2903 – 2913.

[39] Helmut Colfen and Stephen Mann, Angew. Chem. Int. Ed. 2003, 42, 2350 – 2365.

[40] Durham University, http://www.dur.ac.uk/sharon.cooper/lectures/cryskinetics/summary.html, (accessed November 2013).

Figure Captions

Fig. 1. XRPD plot of form I in AS_{P1} and AS_{P2}, and form III in AS_{C3}. The arrow marks indicate the characteristic peak of form I and form III.

Fig. 2. XRPD plot of precipitate obtained in RP_1. The arrow mark denotes the presence of form II in form I.

Fig. 3. Fig. 3. XRPD pattern of CDA crystals grown in SEST method. The inset pattern clearly represents the uniform peak shift to lower angle for powder sample compared with as grown CDA crystals.

Fig. 4. Vibrational spectra of form I and form III.

Fig. 5. (a, b) SEM image of form I crystals obtained from precipitate AS_{P1}. (c) Low (25 μm) and (d) high (10 μm) magnified SEM image of precipitate obtained in AS_{P2}. The circle in the inset figure indicates notches or dimple on the crystal surface.

Fig. 6. Fig.5(a). SEM image of CDA crystal in AS_{C1}. The superstructure formed in edges of form I. Circle and arrow mark indicate the superstructure formed near and/or the uneven or rugged surface (b) Magnified (10 μm) view of flower-like superstructure. The thickness of the petal is about 100 nm.

Fig. 7. (a) Low and (b) high maginified image of form III in AS_{C3}. The red color mark denote the terraces nature of crystal surface (c) optical microscopic image of form III crystals.

Fig. 8. (a) Low and (b) high magnified image of superstructure observed in AS_{C1}. The experiment was conducted at volume fraction of 0.6 with water addition rate 0.4 ml min^{-1}. (c) Observation of flake built form of superstructure.

Fig. 9. SEM image of precipitate obtained at the volume fractions 0.76 (a), 0.83 (b, c) and 0.86 (d) in reprecipitation method. There is no needle crystal observed at 0.76.

Fig. 10. Fig.10. SEM image of superstructure formed in form I crystals obtained in SEST. (a-c) The superstructure was observed in both vertex and edges of the crystals. (d) Flowerlike structure was formed near the uneven or rugged faces.

Fig. 11. Fig.11. (a) Micro sized kinks are observed within the crowed of superstructure. (20 μm-b), (5 μm-c) Magnified view of kink observed in crystals.

Fig. 12. Absorption spectra of AS_{P1} and AS_{C3}. There is no difference in AS_{C3} for pure and mixed solvent.

Table of Contents

Superstructure was formed on form I of 6-chloro-2, 4-dinitroaniline crystals. It was observed in slow evaporation solution growth technique and crystals grown from slow evaporation of filtrate i.e. the mother liquor obtained from anti-solvent precipitation. This flower like superstructure consists of hundreds of square of 2D petals with length and width of several micrometers. The thickness of the petals is about 100 nm.

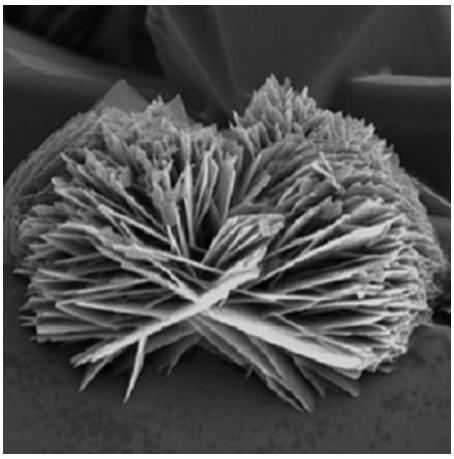

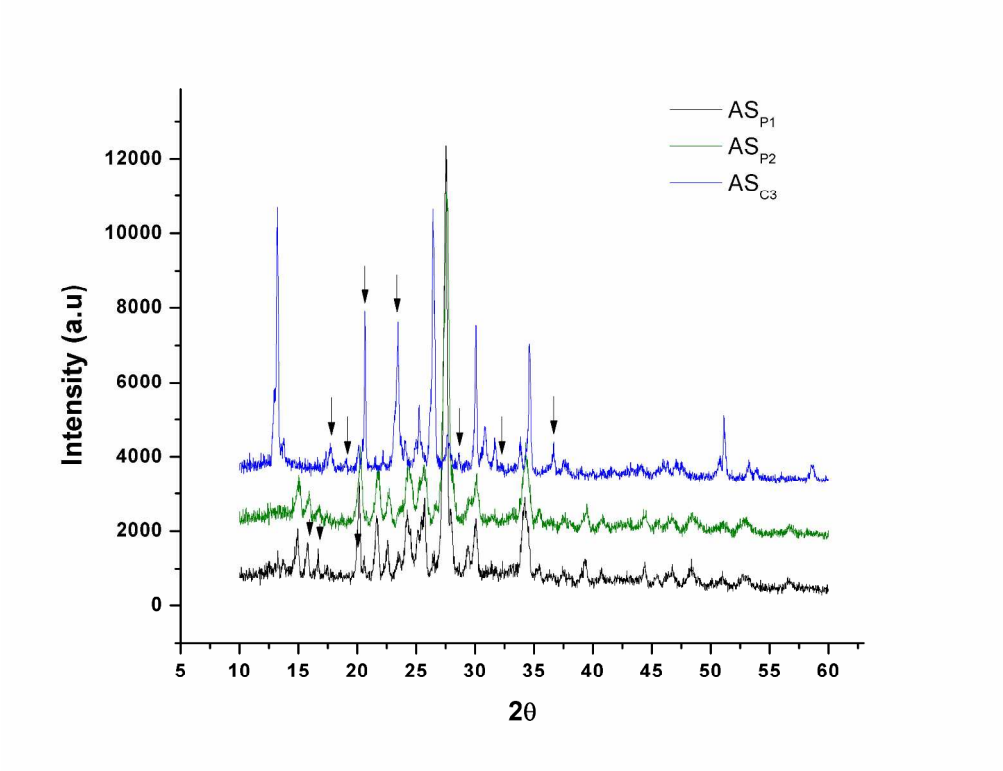

Fig.1
279x215mm (300 x 300 DPI)

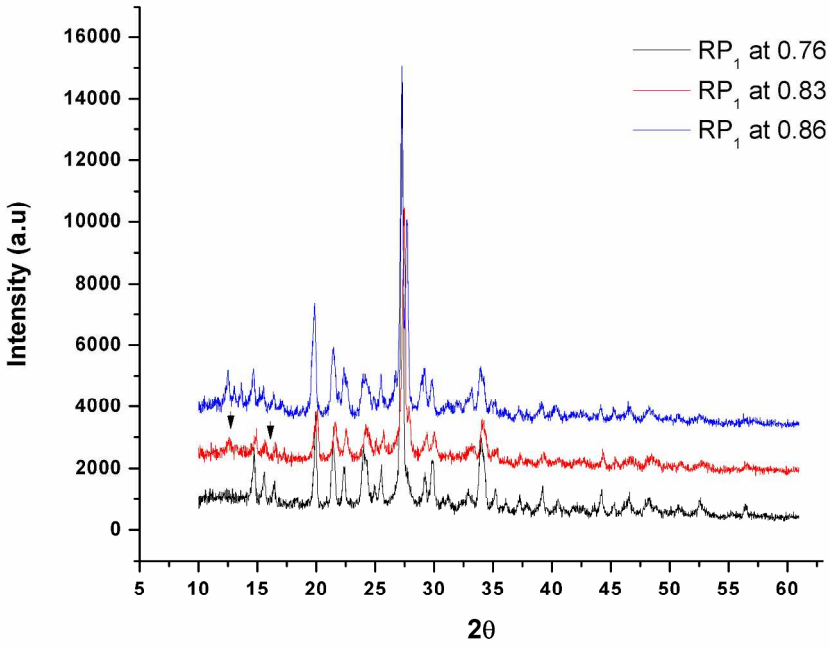

Fig.2
279x215mm (300 x 300 DPI)

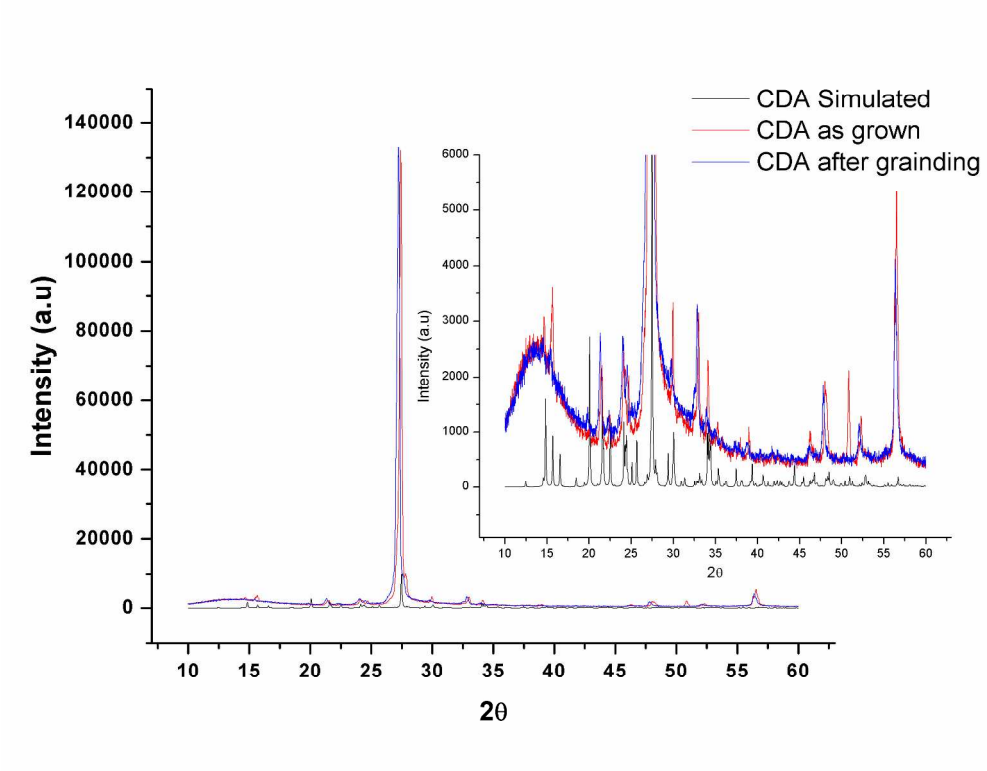

Fig.3
279x215mm (300 x 300 DPI)

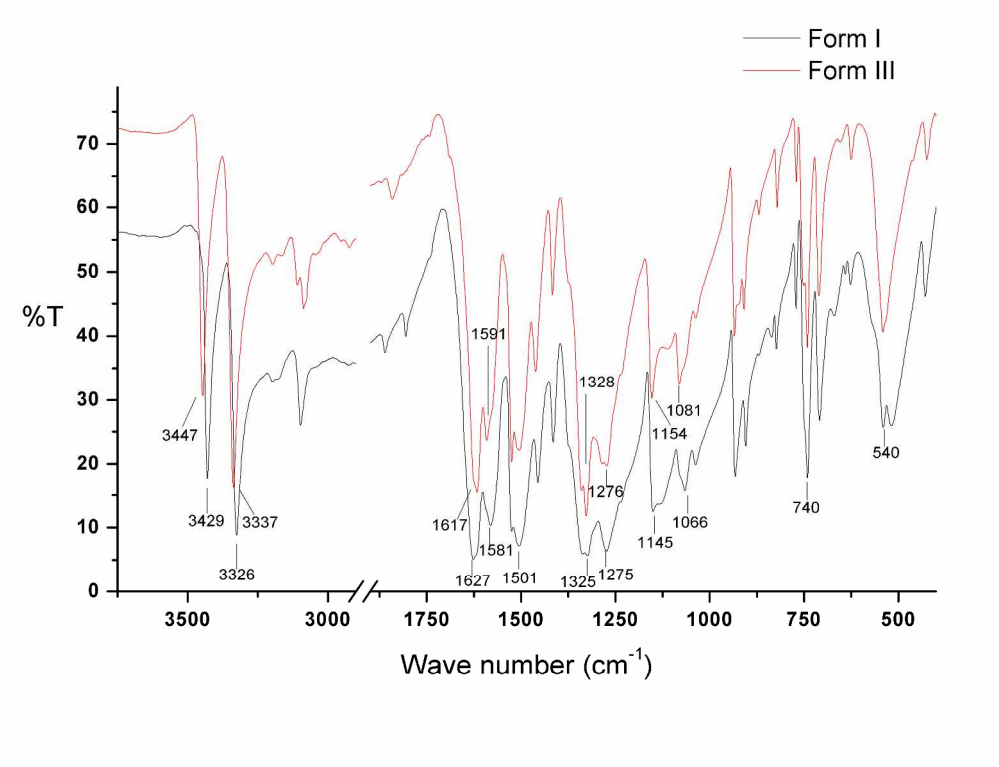

Fig.4
279x215mm (300 x 300 DPI)

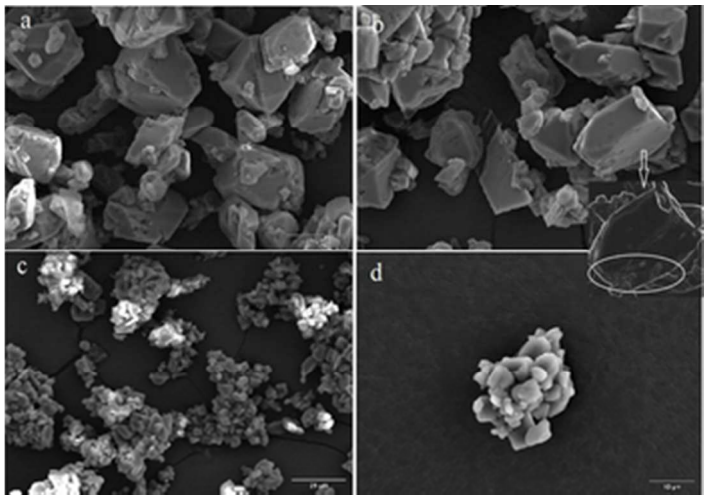

Fig.5
29x20mm (300 x 300 DPI)

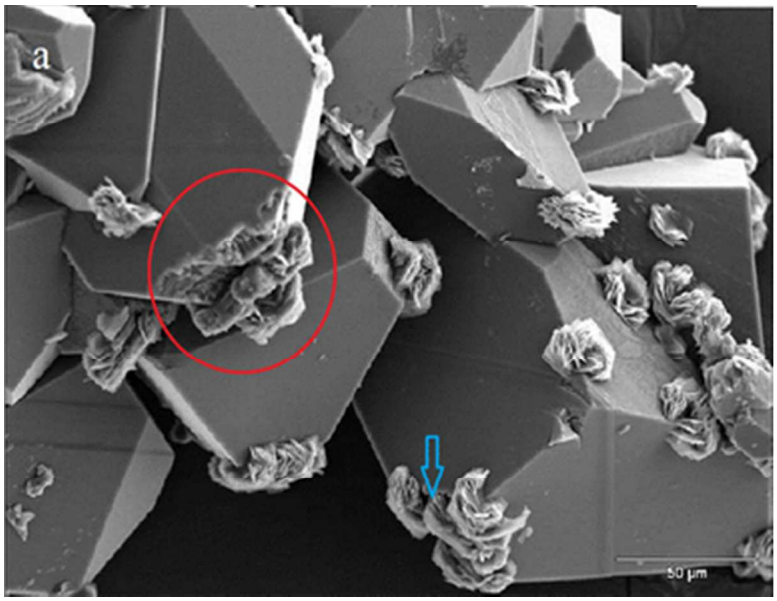

Fig.6a
32x24mm (300 x 300 DPI)

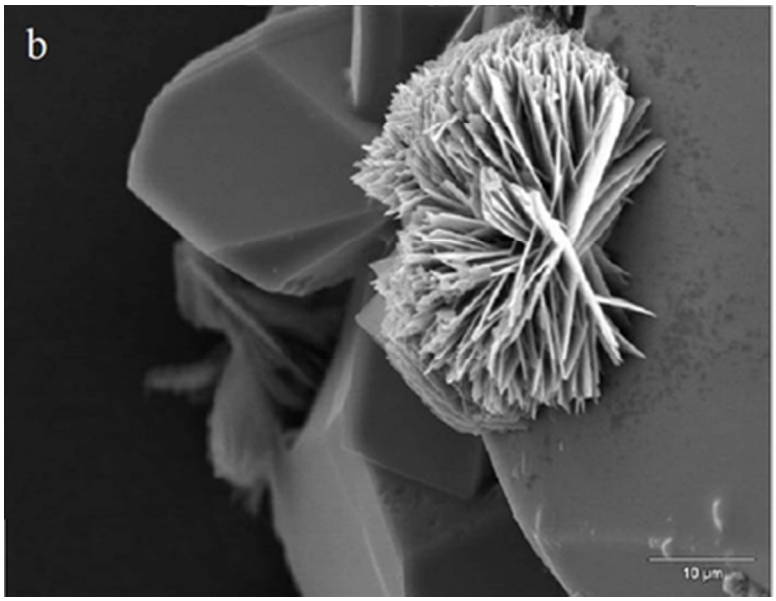

Fig.6b
32x24mm (300 x 300 DPI)

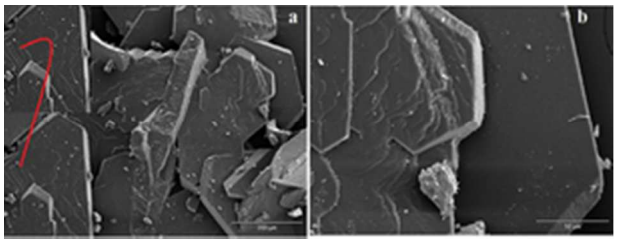

Fig.7ab
25x9mm (300 x 300 DPI)

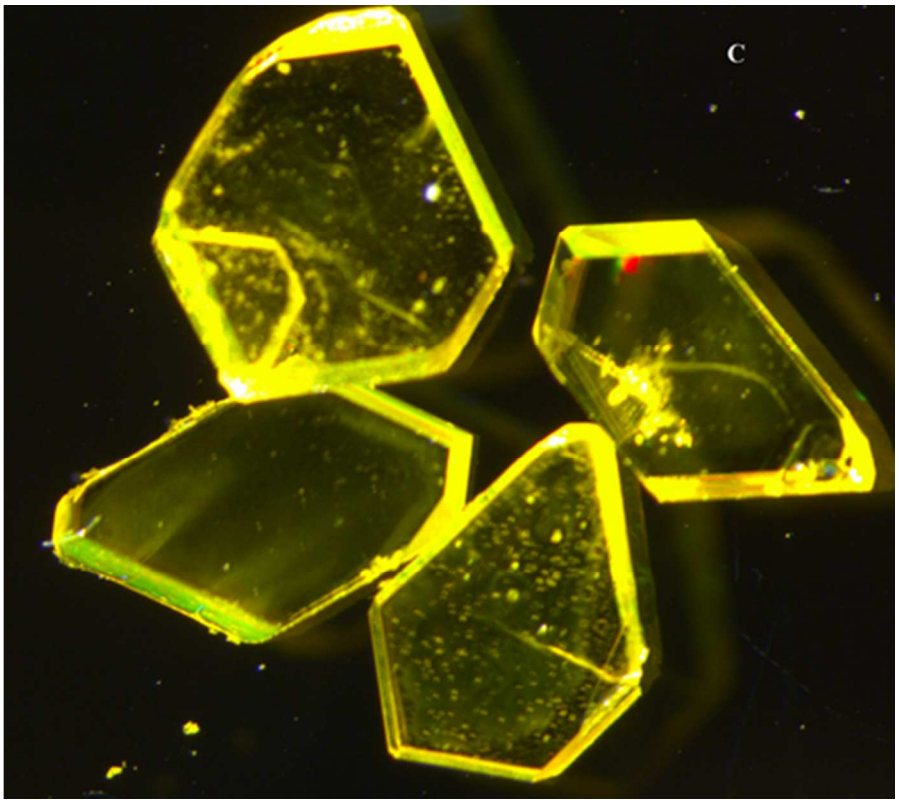

Fig. 7c
37x33mm (300 x 300 DPI)

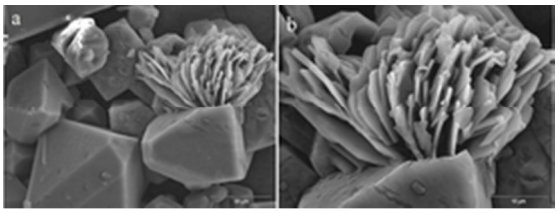

Fig.8ab
23x8mm (300 x 300 DPI)

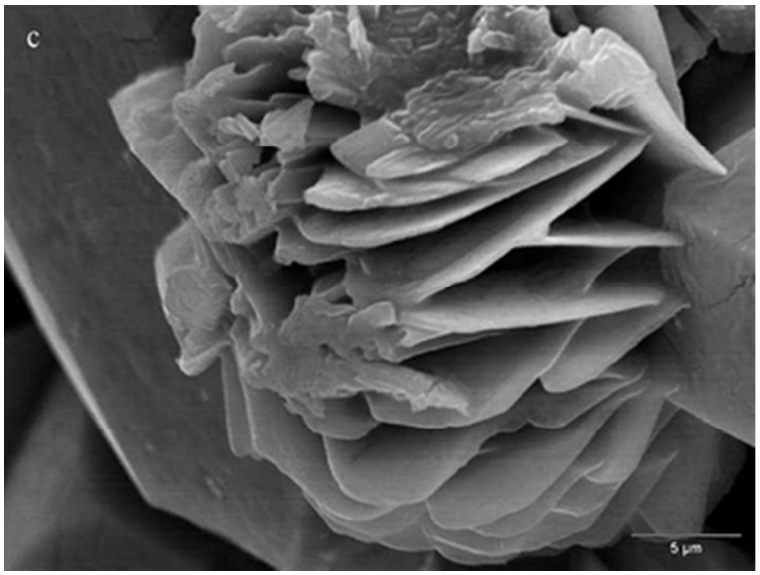

Fig. 8c
31x23mm (300 x 300 DPI)

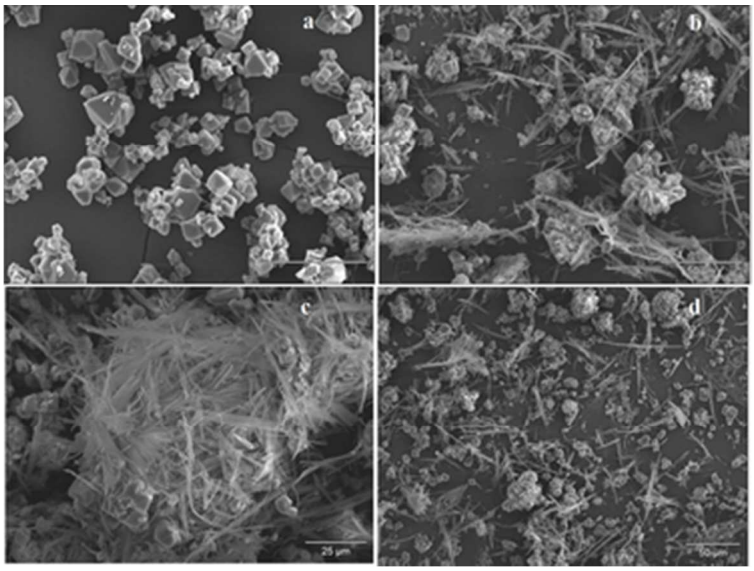

Fig.9
31x23mm (300 x 300 DPI)

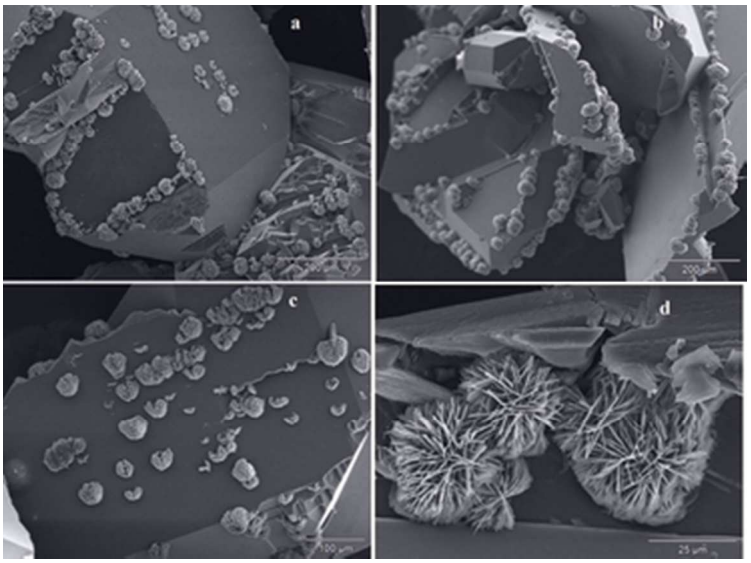

Fig.10
31x23mm (300 x 300 DPI)

Fig.11
15x3mm (300 x 300 DPI)

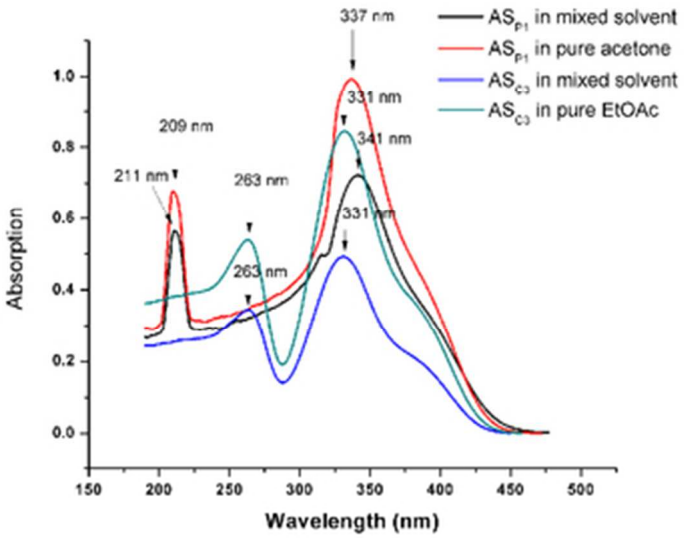

Fig.12
32x25mm (300 x 300 DPI)